AIMS Energy, 11(2): 197–212.
DOI: 10.3934/energy.2023011
Received: 21 September 2022
Revised: 17 February 2023
Accepted: 01 March 2023
Published: 06 March 2023

http://www.aimspress.com/journal/energy

Research article

Conversion of crude palm oil to biofuels via catalytic hydrocracking over NiN-supported natural bentonite

Hasanudin Hasanudin[1,2,*], Wan Ryan Asri[1,2], Utari Permatahati[1,2], Widia Purwaningrum[1,2], Fitri Hadiah[3], Roni Maryana[4], Muhammad Al Muttaqii[4] and Muhammad Hendri[5]

[1] Department of Chemistry, Faculty of Mathematics and Natural Science, Universitas Sriwijaya, Indralaya 30662, Indonesia
[2] Biofuel Research Group, Faculty of Mathematics and Natural Science, Universitas Sriwijaya, Indralaya 30662, Indonesia
[3] Department of Chemical Engineering, Faculty of Engineering, Universitas Sriwijaya, Indralaya 30662, Indonesia
[4] Research Center for Chemistry, Indonesian Institute of Sciences, Building 452 Kawasan PUSPIPTEK, Serpong, Tangerang Selatan, Banten, Indonesia
[5] Department of Marine Science, Faculty of Mathematics and Natural Science, Universitas Sriwijaya, Indralaya 30662, Indonesia

* **Correspondence:** Email: hasanudin@mipa.unsri.ac.id; Tel: +6281367471272.

Abstract: Nickel nitride supported on natural bentonite was prepared and tested for hydrocracking Crude Palm Oil (CPO). The catalyst was prepared using the wet impregnation method and various nickel nitride loading. Subsequently, the nickel nitrate-bentonite was calcined and nitrided under H_2 steam. The surface acidity of as-synthesized NiN-bentonite was evaluated using the gravimetric pyridine gas. Meanwhile, the physiochemical features of the catalyst were assessed using XRD, FT-IR and SEM-EDX. The results showed that the NiN species was finely dispersed without affecting the bentonite's structure. Furthermore, the co-existence of Ni and N species on EDX analysis suggested the NiN was successfully supported onto the bentonite, while the surface acidity features of raw bentonite were increased to 1.713 mmol pyridine/g at 8 mEq/g of nickel nitride loading. The catalytic activity towards the CPO hydrocracking demonstrated that the surface acidity features affect the CPO conversion, with the highest conversion achieved (84.21%) using NiN-bentonite 8 mEq/g loading. At all nickel nitride loading, the NiN-bentonite could generate up to 81.98–83.47% of bio-kerosene fraction, followed by the bio-gasoline ranging from 13.12–13.9%, and fuel oil ranging from 2.89–4.57%.

Keywords: hydrocracking; crude palm oil; nickel nitride; supported natural bentonite; biofuels

1. Introduction

Due to the escalation of industrial activities worldwide, energy needs are increasing every year. This condition is consistent with the significant increase in population and economic development [1]. Fossil fuels have been the main focus in many industrial processes, as well as in automobiles. Globally, the development of cleaner and renewable energy sources is accelerating due to sharp rises in crude oil costs, the depletion of petroleum supplies and the environmental consequences of emissions [2]. Indonesia, in particular, offers enormous potential for clean, renewable energy use. Crude Palm Oil (CPO) is one of the natural resources with a supply that can be used as an alternative energy [3]. In recent years, CPO manufacturing rose to 27.00 million tonnes in 2017 compared with 2001, which is only 0.84 million tonnes. Further, CPO manufacture's productivity tends to increase yearly by 1.50–10.96%, which suggests its potential as a sustainable feedstock [4].

CPO is made up of triglycerides and fatty acids that can be converted into sustainable fuels by hydrocracking [5]. This reaction uses hydrogen gas and a solid acid catalyst to break long-chain hydrocarbon bonds into short-chain hydrocarbons [6]. The type of solid acid catalyst must be investigated because it has a direct impact on the conversion. Acid catalysts are widely employed in petrochemical reactions and industrial biomass conversion [7,8]. The properties of the catalyst also could be tunable for particular raw material and outcomes. Solid acid, a well-known heterogeneous catalyst, has been extensively explored to generate green and sustainable chemistry due to its high catalytic activity and product selectivity, ease of regeneration and corrosion reduction, and ability to function in continuous reactors [9,10].

Currently, the metal-based catalyst can be utilized for hydrocracking reactions. However, the main disadvantage of metal-based catalysts in hydrocracking processes is low surface area and proclivity to agglomeration. To compensate for this weakness, a supported catalyst with a wide surface area and an active catalytic site is required [11]. Several supported metal acids, such as Al_2O_3-SiO_2 [12], zeolite [13,14], MCM-41 [15,16], TiO_2-SiO_2 [17] and bentonite [18–20] have been utilized as hydrocracking reaction supported catalysts for producing biofuels. All these support catalysts are impregnated with an active metal, such as Ni-W, Ni, Ni-1,3,5-benzenetricarboxylate (Ni-BTC), NiMo, NiMoS, NiWS and Ni-Cu, for the hydrogenation facility.

In the context of a support catalyst, natural bentonite is very promising, as it reveals superiority because it is abundantly available, can co-exists in Bronsted and Lewis acid sites [21], and the structure, as well as pores, can be straightforwardly modified [22]. Several studies showed that natural bentonite's catalytic and physiochemical features could be enhanced by adding active species, such as metal-based catalysts, to the bentonite's surface or matrix catalyst [19,23]. This treatment could promote the acidity and textural features of bentonite, which affects the hydrocracking process [24,25].

Currently, there is much interest in the metal transition nitride due to its attractive physicochemical features, as this catalyst has many potential applications [26–28]. Many metal nitride-based catalysts, such as ScN, VN, TiN, CrN, FeN, CoN and NiN have been extensively explored and used for various purposes [29,30]. Previous studies revealed that the modification of natural bentonite using MoN and ZrN positively affected the hydrocracking activity [3,31]. ZrN/bentonite exhibited high acidity features (1.822 mmol/g) compared with the parent bentonite, with only 0.054 mmol/g.

Notably, the NiN catalyst is fascinating due to its high specific surface area, flexible catalytic features, being relatively inexpensive and abundantly available, once compared with noble metal-based catalysts [32,33]. Accumulation of positive charge on the Ni sites with N substance alloying, the ΔG_{H^*} in the favored NiN plane decreases significantly to −0.05 eV, almost close to the Pt sites [34]. Hence, dispersing the NiN onto the supported catalyst, such as bentonite, would potentially increase the active site catalyst, thereby increasing catalytic performance.

According to the literature review, the NiN catalyst has been utilized for the electrochemical reaction [27,28,33,35,36]. However, their potential application for CPO hydrocracking was limited. In this study, the NiN supported-natural bentonite was prepared, and its catalytic activity towards the hydrocracking of CPO was assessed. This study offers the potential and exploration of natural-based catalysts as inexpensive catalysts. Nickel nitride, as an active species, was studied to evaluate its effect on the natural bentonite catalyst in order to increase its catalytic performance on CPO hydrocracking. This catalyst would provide alternative acidic sites, enhancing the catalytic activity of natural bentonite towards CPO hydrocracking. The effect of NiN loading on the hydrocracking of CPO conversion and their selectivity towards biofuels was evaluated. Furthermore, the physicochemical of natural bentonite and NiN-supported natural bentonite catalyst was assessed using XRD, FTIR, and SEM-EDX, while the surface acidity features were evaluated with the gravimetric method using pyridine gas.

2. Materials and methods

2.1. Synthesis of NiN-Bentonite

The as-saturated Na-bentonite (Na-B) (Bayan, Central java) was first prepared according to that previously reported [21]. The wet impregnation method was employed for the Na-B modification using nickel solution ($NiCl_2.6H_2O$, ≥99.0% purity, Merck). Briefly, 5 g of Na-B was dispersed to the 0.1 M of nickel solution, and 1 M of ammonium nitrate solution was gradually added (1 mL/min) (NH_4NO_3, ≥ 95.0% purity, Merck), and stirred for 1 h at room temperature (RT). In this process, the volume of nickel solution and ammonium solution varied with different loading, i.e., 2, 4, 6, 8, 10 mEq/g. Afterwards, the solution was stirred for 24 h, and the temperature was increased to 80 ℃ until it formed a paste. The paste was cleaned with distilled water and dried for 24 h at 105 ℃. Subsequently, the dried solid was later calcined at 550 ℃ for 3 h, and then reduced under an H_2 atmosphere at 600 ℃ for 2 h.

2.2. Characterization of catalysts

The morphology and elemental composition of both the parent Na-B and NiN-B samples were investigated on SEM-EDX JEOL JSM 650. Rigaku Mini Flex 600 and FTIR 8201 resolved the structure and functional groups of catalysts. Based on the previously reported, the pyridine vapour gravimetric method was employed for the catalysts' surface acidity analysis [21].

2.3. Catalytic activity test

The hydrocracking was conducted in the continuous fixed bed microreactor [37]. The H_2 gas was first supplied to the reactor to remove the oxygen gas. A peristaltic pump was used to maintain a CPO feed flow of 11.94 g/min and 12 g of catalyst. The CPO hydrocracking was conducted at 450 ℃ and

held for 0.12 h with an H_2 gas flow of 2 mL/s. Furthermore, the condensable liquid product was vacuum distilled at 200 ℃. The residue after vacuum distillation was separated, and the liquid product was analyzed using GC-MS (Thermo Scientific). The total conversion of CPO was determined based on Eq (1) as follows:

$$\text{Conversion } (\%) = \frac{X_o - X}{X_o} \times 100\%, \quad (1)$$

where X_o and X are the weight of feed and unreacted feed, respectively.

3. Results and discussion

3.1. Catalyst characterization

Various techniques were used to characterize the prepared Na-B and NiN-B. Figure 1 depicts the diffractograms of both catalysts. As can be discerned in Figure 1a, the diffraction peaks at 2θ of 19.70˚, 25.66˚, 33.72˚, 55.33˚ and 62.21˚ were assigned as typical of montmorillonite mineral [38]. These montmorillonite mineral peaks were also consistently observed by another study [39]. According to Huang et al. [40], montmorillonite's distinctive reflection was indicated by low angle 2 in clay-based materials. Figure 1b shows that this high peak intensity at 5.27˚ was quite unobservable after being loaded with nickel nitride. This condition occurred, presumably, due to delamination of the silicate layer, which was known as the unique feature in the clay-based material and could lead to the formation of a house of cards structure [41]. Similar findings were also reported by the previous study, which revealed the disappearance of 2θ at 5.96˚ of montmorillonite after being modified by ZrO_2 and Ni/Mo-ZrO_2 [42].

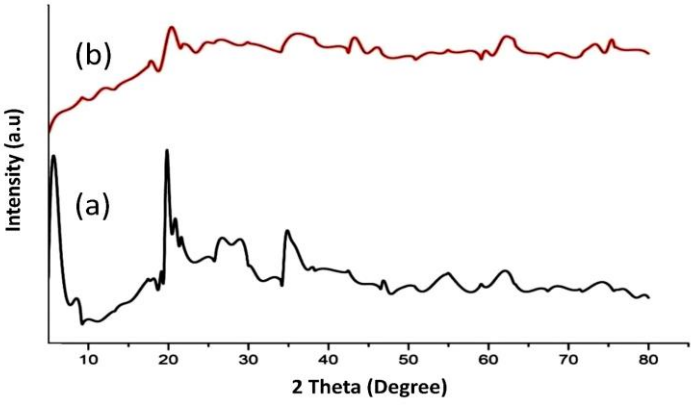

Figure 1. Diffractograms of (a) bentonite and (b) nickel nitride-bentonite.

As shown in Figure 1b, a typical montmorillonite phase still existed in the NiN-B, suggesting that NiN did not negatively amend the bentonite structure [43]. Other studies reported [27,30,44] that the nickel nitride phase was difficult to discriminate against the parent Na-B. The NiN phase's unnoticeable peaks on modified bentonite likely indicated that the NiN was evenly distributed across the surface of the bentonite [45]. Furthermore, there was an intensity change and peak shift on the

NiN-B, probably due to the disproportionate ionic size between natural bentonite and nickel nitride ions. This observation was also reported by Olegario et al. [46] during the modification of Philippine natural zeolite using iron and copper metal oxide.

Figure 2 shows the FTIR spectra of the parent Na-B and NiN-B. The absorption band of Na-B at 3390, 3615, and 1623 cm^{-1} were assigned as the hydroxyl group deformation of water [47]. These peaks on Na-B can also correspond to the stretching vibration of a hydroxyl group from silanol, as well as Al-OH groups [48]. The bands at 984 and 795 cm^{-1} indicated the Si-O-Si and Si-O-Al stretching and deformation bands from the phyllosilicate groups on the bentonite [49]. Other studies also observed these typical absorption bands of bentonite [50].

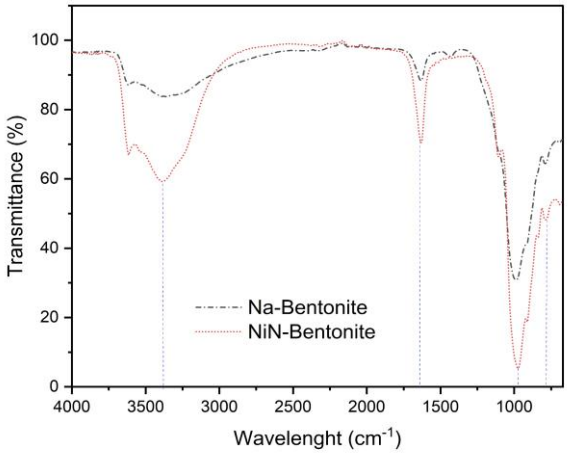

Figure 2. FTIR spectra of bentonite and nickel nitride-bentonite.

Due to the overlap between the bentonite's structural elements, the nickel species absorption bands on the NiN-B were largely unobserved. This condition was also reported coherently during the modification of bentonite using different species Al/Fe and Fe [43,51]. The presence of NiN is likely what caused the phyllosilicate group absorption band on the NiN-B to shift relative to a higher wavelength and gain intensity noticeably similar to other bands. Mishra et al. [52] reported the same phenomenon, revealing that the modification of bentonite with CTAB to organo-bentonite resulted in a shift in absorption towards the higher wavelength. According to Tomul et al. [53], the increase in the intensity of the air bending vibration suggested the rise in air storage capacity and the acidity feature of modified bentonite, due to the generation of a proton by the H_2O molecular dissociation in the coordination plane.

Figure 3 shows the SEM micrograph of Na-B and NiN-B. It can be seen that the parent Na-B had a layered surface structure and an asymmetrical irregularly particle shape. This was typical of bentonite surfaces and other as-prepared raw bentonites from previous studies [54–56]. There was no appreciable surface change on the NiN-B compared with the parent Na-B. The Na-B modification using NiN species did not notably influence the bentonite's morphology, which was consistent with the previous XRD and FTIR results. Vajglová et al. also reported a similar finding [57] by modifying the bentonite using Pt through the impregnation method. Some studies reported that the modified bentonite exhibited a more porous and coarse structure [58,59]. Nevertheless, it was worth noting that some tiny

aggregation species were deposited on the NiN-B, presumably contributing to NiN species' dispersion towards the bentonite surface. Lin et al. [60] reported that the emergence of particle aggregates on Zr-bentonite, compared with raw bentonite, suggested the success of Zr loaded on the bentonite's surface.

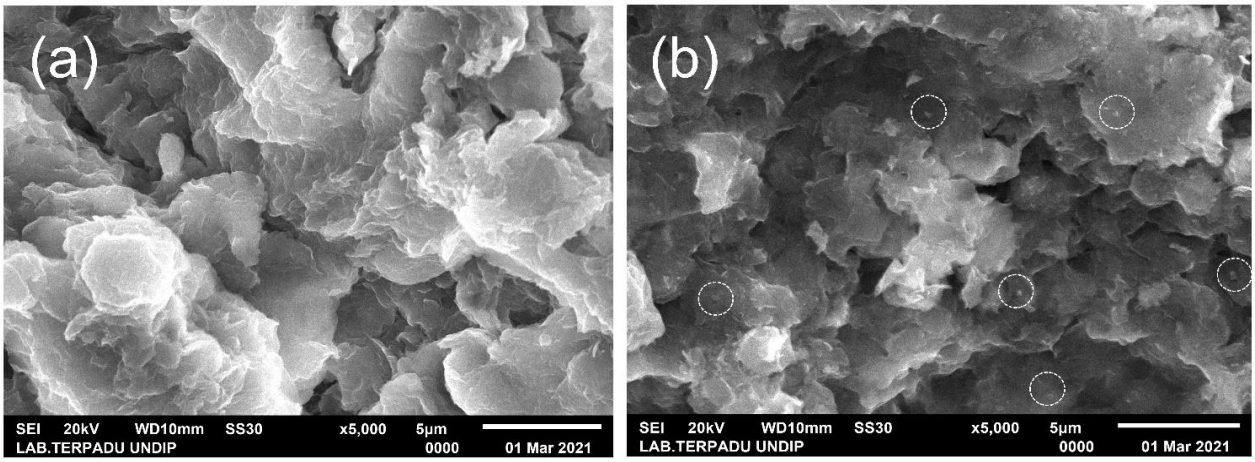

Figure 3. SEM micrographs of (a) bentonite and (b) nickel nitride-bentonite.

Table 1 and Figure 4 presents the semiquantitative EDX analysis of Na-B and NiN-B. The Na-B consisted of Si, Al, Mg, Na, C and Fe, as well as other impurities, and these components were also reported by other studies [61,62]. Also, the co-existence of nickel (13.19 wt%) and nitrogen (3.23 wt%) in NiN-B confirmed the successful modification of bentonite with NiN species. The Si/Al ratio of the Na-B was relatively unchanged by NiN, suggesting that bentonite's layer structure was well maintained during modification [53].

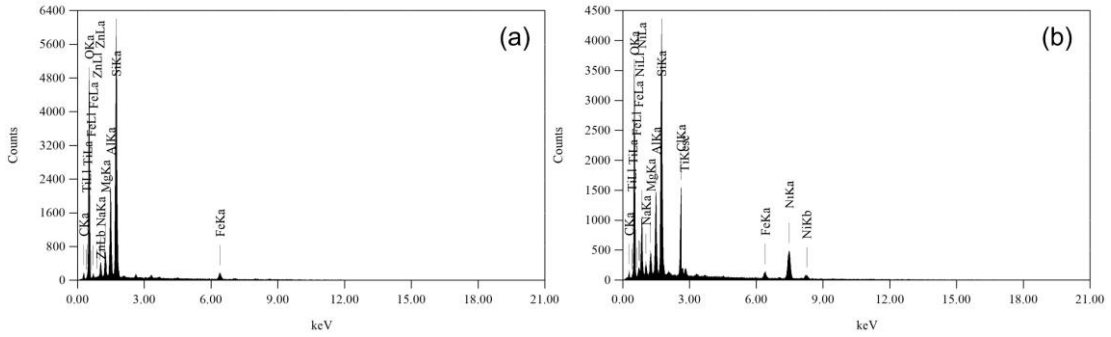

Figure 4. EDX spectra of (a) bentonite and (b) nickel nitride-bentonite.

Table 1. EDX results of bentonite and nickel-nitride bentonite.

Element	Atomic (wt%)	
	Na-B	NiN-B
Si	25.13	18.39
Al	8.11	6
Ni	0	13.19
N	0	3.23
Na	1.81	1.57
Mg	2.01	1.01
Ca	0.29	0.19
O	39.24	35.5
Fe	3.12	2.07
C	16.18	15.09
Zn	1.3	1.2
Fe	1.2	1.13
Ti	0.38	0.21
Cl	1.23	1.22

Figure 5 shows the surface acidity features of Na-B and NiN-B with different loading. The Na-B had a relatively low surface acidity of 0.086 mmol pyridine/g compared with NiN-B 2 mEq/g of 0.721 mmol pyridine/g. This indicated that the NiN species positively affected the surface acidity of the parent natural bentonite by providing both new Lewis and Bronsted acidic sites, raising the surface acidity of Na-B. Furthermore, the interaction of nickel with nitrogen in metal-nitride compounds facilitates a more significant enlargement in electron density [63], which directly affects the surface acidity of the catalyst. The previous study also reported that the total acidity of raw bentonite could be increased by using MoP species [21].

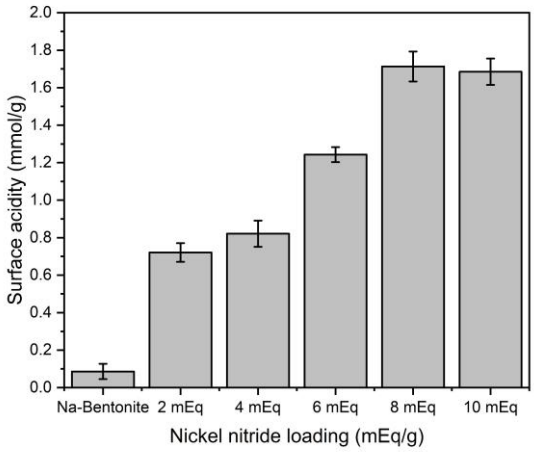

Figure 5. The surface acidity of bentonite and nickel nitride-bentonite.

Moreover, as the nickel nitride loading increased, the surface acidity of the NiN-B catalyst also increased. The previous study also consistently noticed this metal-nitride acidity features trend [31]. As shown in Figure 5, the highest surface acidity was accomplished by loading 8 mEq/g nickel nitride with a surface acidity of 1.713 mmol pyridine/g. However, a low nickel loading (10 mEq/g) reduced the surface acidity of the catalysts to 1.685 mmol pyridine/g. This condition was most likely caused by catalyst agglomeration, which reduced adsorption efficiency towards the pyridine probe and, thus, surface acidity. The decrease of acidity features at 10 mEq/g metal loading was also observed on the ZrN-bentonite [3].

3.2. Catalytic activity test

The hydrocracking was performed using the continuous fixed bed microreactor over the NiN-B catalyst with different nickel nitride loading. The measurements were recorded in triplicates, and the results were shown as a mean value. Figure 6 shows conversion results using bentonite and NiN-B catalysts. The parent bentonite catalyst exhibited low conversion compared with the NiN-B catalyst, which is suggested to be due to low acidic sites. The NiN-B with 2 mEq/g nickel nitride loading generated up to 65.4% CPO conversion and increased the nickel nitride loading gradually this process. According to Figure 6, the highest conversion was generated by 8 mEq/g nickel nitride loading of 84.21%, while an insignificant decrease was observed on 10 mEq/g nickel nitride loading. This result confirms that the NiN species could enhance the bentonite catalyst performance toward high CPO conversion.

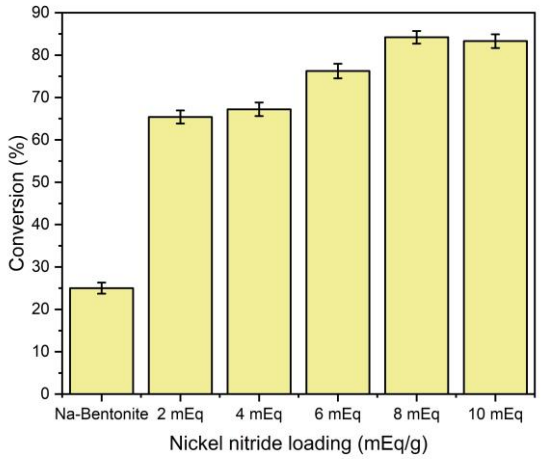

Figure 6. Effect of nickel nitride-bentonite catalyst with different loading on CPO conversion.

It has been reported that the vegetable oil conversion through the hydrocracking reaction is inherently affected by the catalyst's acidity [31]. These Lewis and Bronsted acid sites are crucial in the hydrogenation process, including the production of reactive carbocations [64]. Furthermore, the higher nickel nitride loading provided a more acidic environment on the catalyst's surface throughout the synergetic effect between nitride groups and metal. This condition effectively promoted the CPO conversion [65]. As can be seen from Figure 6, higher nickel nitride loading provided highly acidic sites, which promoted a high catalytic process. Similarly, the previous study showed that ZrN-bentonite

could exhibit a conversion of up to 87.93% at 8 mEq/g metal loading, while the ZrP-bentonite achieved 86.04% at 10 mEq/g metal loading, which indicated that the catalyst acidity highly affected the CPO conversion [3]. Another study also reported a positive correlation between the catalyst acidity and the catalytic performance in the hydrocracking process [66]. According to a previous study, CoMo-supported alumina catalyst exhibited a conversion of 64.21% during a 2 h hydrocracking at 400 ℃ [67], while NiW-supported HZSM-5 generated 48.16% at 350 ℃ for 1 h reaction [68]. The CPO that has not yet undergone prosperous cracking is denoted as residue. According to the results of the CPO hydrocracking, the parent catalyst exhibited high residue, whereas the nickel nitride-bentonite showed low residue, and tended to decrease for prolonged high nickel nitride loading, which was proportional with high conversion. The low residue result suggested that the catalyst was effective for CPO hydrocracking [69].

Figure 7 shows biofuel fractions resulting from the NiN-B with the different nickel nitride loading. Employing various nickel nitride loading resulted in no significant difference in the biofuel fractions. This suggested that the acidity concentration likely had no strong correlation with the quantity of each biofuel fraction [70]. Instead, hydrocracking parameters, such as temperature, might likely affect biofuel distribution. It can be seen that, among the nickel nitride loading, the bio-kerosene had a higher fraction (81.98–83.47%), followed by the bio-gasoline (13.12–13.9%) and fuel oil (2.89–4.57%).

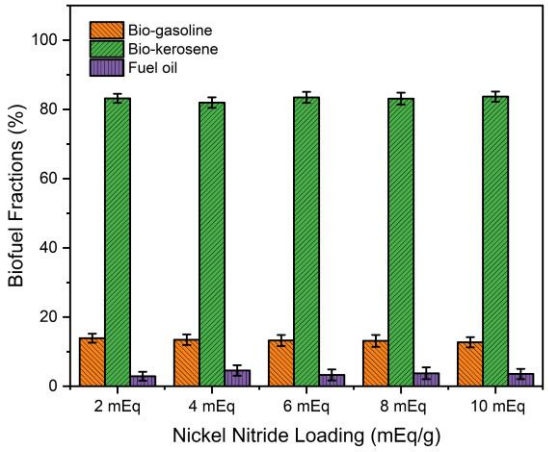

Figure 7. The biofuel fractions of CPO hydrocracking using nickel nitride-bentonite.

In this reaction, the fatty acid glycerol ester linkages disintegrate into free fatty acids. The hydrogenation reaction is involved in the creation of bio-kerosine. Concurrently, the decarboxylation reaction begins with the active catalyst site contacting fatty acids through the oxygen atom adsorption on the carboxyl groups of fatty acids. The bio-kerosene fraction is produced in large amounts under these conditions [3]. Meanwhile, the bio-gasoline portion was made by additional hydrocracking of the bio-kerosene. Heavy fractions, such as fuel oil, were generated from insufficient cracking or coupling reactions. The previous study reported that ZrN-bentonite could achieve a bio-kerosene fraction of ca. 72–75% and bio-gasoline fraction of ca. 21–22%, while ZrP-bentonite could generate the bio-kerosene and bio-gasoline fractions of ca. 74–83% and ca. 6.8-14%, respectively [3]. Furthermore, MoN-bentonite 8 mEq/g metal loading could exhibit a bio-gasoline fraction of up to 28.7% [31]. Based

on the hydrocracking investigation, the NiN-B catalyst showed an acceptable performance towards biofuel production through the CPO hydrocracking compared with other supported bentonite catalysts. The proposed mechanism of CPO hydrocracking using nickel nitride-bentonite is presented in Figure 8. The CPO hydrocracking process can occur as a result of a parallel reaction between the decarboxylation reaction and the carbon-carbon bond-breaking reaction of unsaturated fatty acids. This parallel reaction allows the formation of carbon dioxide gas products and gasoline fraction oil. This reaction, likewise, begins with the adsorption of unsaturated fatty acids as a provider of electrons to the catalyst surface as an electron acceptor. The weak bonds formed between fatty acids that have phi electrons (π) and, subsequently, the catalyst, led the carbon-carbon bonds of unsaturated fatty acids to become weak and eventually break. Further hydrogenation reactions generated gases, such as propane, biofuel fractions and water.

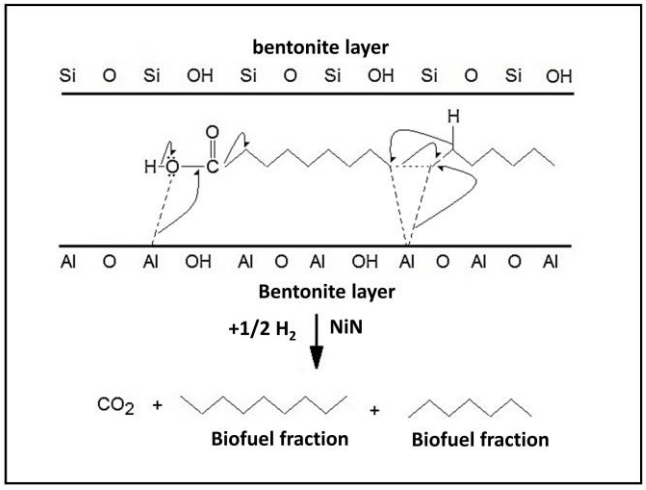

Figure 8. The proposed mechanism of CPO hydrocracking using nickel nitride-bentonite.

4. Conclusions

A series of NiN-bentonite with varying nickel nitride loading was prepared, and their catalytic activity towards the CPO hydrocracking was evaluated. By using the wet impregnation method and nickel solution, as well as ammonium solution as the nickel and nitrogen precursors, respectively, the natural bentonite was modified with NiN species. Also, the as-prepared catalyst was calcined and reduced under an H_2 atmosphere. According to the catalyst's characterizations, the NiN species was sufficiently supported on the surface of the bentonite. Moreover, the surface acidity of the parent natural bentonite was enhanced, with the highest acidity of up to 1.713 mmol pyridine/g achieved by the 8 mEq/g of nickel nitride loading. The hydrocracking catalytic test revealed that the NiN-bentonite with 8 mEq/g exhibited up to 84.21% CPO conversion, with a bio-gasoline fraction of 13.12%, bio-kerosene of 83.12 and a fuel oil of 3.76%. This catalyst provides a potential application for CPO hydrocracking with adequate performance.

Acknowledgments

The financial support by The LPPM Universitas Sriwijaya under Hibah Kompetitif scheme research grant 2022 No. 0109/UN9.3.1/SK/2022 is gratefully acknowledged. The authors also acknowledge the National Research and Innovation Agency (BRIN) for providing access to instrumental analysis.

Conflict of interest

We declare no conflicts of interest.

References

1. Sari EP, Wijaya K, Trisunaryanti W, et al. (2022) The effective combination of zirconia superacid and zirconia-impregnated CaO in biodiesel manufacturing: Utilization of used coconut cooking oil (UCCO). *Int J Energy Environ Eng* 13: 967–978. https://doi.org/10.1007/s40095-021-00439-4
2. Wijaya K, Saputri WD, Aziz ITA, et al. (2022) Mesoporous silica preparation using sodium bicarbonate as template and application of the silica for hydrocracking of used cooking oil into biofuel. *Silicon* 14: 1583–1591. https://doi.org/10.1007/s12633-021-00946-3
3. Hasanudin H, Asri WR, Zulaikha IS, et al. (2022) Hydrocracking of crude palm oil to a biofuel using zirconium nitride and zirconium phosphide-modified bentonite. *RSC Adv* 12: 21916–21925. https://doi.org/10.1039/d2ra03941a
4. Hasanudin H, Asri WR, Muthiarani TE, et al. (2022) Esterification of free fatty acid from sludge palm oil using zeolite-sulfonated carbon from sugar cane catalysts. *J Oil Palm Res*. In Press. https://doi.org/10.21894/jopr.2022.0051
5. Istadi I, Riyanto T, Khofiyanida E, et al. (2021) Low-oxygenated biofuels production from palm oil through hydrocracking process using the enhanced Spent RFCC catalysts. *Bioresour Technol Rep* 14: 100677. https://doi.org/10.1016/j.biteb.2021.100677
6. Rasyid R, Malik R, Kusuma HS, et al. (2018) Triglycerides hydrocracking reaction of nyamplung oil with non-sulfided CoMo/γ-Al_2O_3 Catalysts. *Bull Chem React Eng Catal* 13: 196–203. https://doi.org/10.9767/bcrec.13.2.734.196-203
7. Wu Q, Liu F, Yi X, et al. (2018) A solvent-free, one-step synthesis of sulfonic acid group-functionalized mesoporous organosilica with ultra-high acid concentrations and excellent catalytic activities. *Green Chem* 20: 1020–1030. https://doi.org/10.1039/c8gc00002f
8. Liu F, Huang K, Zheng A, et al. (2018) Hydrophobic solid acids and their catalytic applications in green and sustainable chemistry. *ACS Catal* 8: 372–391. https://doi.org/10.1021/acscatal.7b03369
9. Liu F, Yi X, Chen W, et al. (2019) Developing two-dimensional solid superacids with enhanced mass transport, extremely high acid strength and superior catalytic performance. *Chem Sci* 10: 5875–5883. https://doi.org/10.1039/c9sc01988j
10. Peng WL, Mi J, Liu F, et al. (2020) Accelerating biodiesel catalytic production by confined activation of methanol over high-concentration ionic liquid-grafted UiO-66 solid superacids. *ACS Catal* 10: 11848–11856. https://doi.org/10.1021/acscatal.0c03261

11. Hasanudin H, Asri WR, Meilani A, et al. (2022) Kinetics study of free fatty acid esterification from sludge palm oil using zeolite sulfonated biochar from molasses composite catalyst. *Mater Sci Forum* 1061: 113–118. https://doi.org/10.4028/p-5ovu3d
12. Anand M, Farooqui SA, Kumar R, et al. (2016) Optimizing renewable oil hydrocracking conditions for aviation bio-kerosene production. *Fuel Process Technol* 151: 50–58. https://doi.org/10.1016/j.fuproc.2016.05.028
13. Susi EP, Wijaya K, Wangsa, et al. (2020) Effect of nickel concentration in natural zeolite as catalyst in hydrocracking process of used cooking oil. *Asian J Chem* 32: 2773–2777. https://doi.org/10.14233/ajchem.2020.22708
14. Kadarwati S, Rahmawati F, Eka Rahayu P, et al. (2013) Kinetics and mechanism of Ni/zeolite-catalyzed hydrocracking of palm oil into bio-fuel. *Indones J Chem* 13: 77–85. https://doi.org/10.22146/ijc.21330
15. Zhu Y, Zhang Z, Cheng J, et al. (2021) Ni-BTC metal-organic framework loaded on MCM-41 to promote hydrodeoxygenation and hydrocracking in jet biofuel production. *Int J Hydrogen Energy* 46: 3898–3908. https://doi.org/10.1016/j.ijhydene.2020.10.216
16. El-Deeb ZM, Aboutaleb WA, Mohamed RS, et al. (2022) Gasoline and diesel-like fuel production via hydrocracking of hydrotreated tire pyrolytic oil over Ni-W/MCM-41 derived from blast furnace slag. *J Energy Inst* 103: 84–93 https://doi.org/10.1016/j.joei.2022.05.013
17. Lee J, Hwang S, Lee SB, et al. (2010) Production of middle distillate through hydrocracking of paraffin wax over NiMo/TiO_2-SiO_2 catalysts. *Korean J Chem Eng* 27: 1755–1759. https://doi.org/10.1007/s11814-010-0279-3
18. Wijaya K, Kurniawan MA, Saputri WD, et al. (2021) Synthesis of nickel catalyst supported on ZrO_2/SO_4 pillared bentonite and its application for conversion of coconut oil into gasoline via hydrocracking process. *J Environ Chem Eng* 9: 105399. https://doi.org/10.1016/j.jece.2021.105399
19. Suseno A, Wijaya K, Trisunaryanti W (2018) Synthesis and characterization of Ni-Cu doped zirconia-pillared bentonite. *Orient J Chem* 34: 1427–1431. http://doi.org/10.13005/ojc/340332
20. Cortés JC, Rodríguez C, Molina R, et al. (2021) Hydrocracking of 1-methylnaphtalene (1MN) over modified clays-supported NiMoS and NiWS catalyst. *Fuel* 295: 120612. https://doi.org/10.1016/j.fuel.2021.120612
21. Hasanudin H, Asri WR, Tampubolon K, et al. (2022) Dehydration isopropyl alcohol to diisopropyl ether over molybdenum phosphide pillared bentonite. *Pertanika J Sci Technol* 30: 1739–1754. https://doi.org/10.47836/pjst.30.2.47
22. Mofrad BD, Hayati-Ashtiani M, Rezaei M (2018) Preparation of pillared nanoporous bentonite and its application as catalyst support in dry reforming reaction. *Asia-Pacific J Chem Eng* 13: 1–11. https://doi.org/10.1002/apj.2188
23. Wijaya K, Ariyanti AD, Tahir I, et al. (2018) Synthesis of Cr/Al_2O_3-bentonite nanocomposite as the hydrocracking catalyst of castor oil. *Nano Hybrids Compos* 19: 46–54. https://doi.org/10.4028/www.scientific.net/nhc.19.46
24. Mirzan M, Wijaya K, Falah II, et al. (2019) Synthesis and characterization of Ni-promoted zirconia pillared bentonite. *J Phys Conf Ser* 1242: 012013. https://doi.org/10.1088/1742-6596/1242/1/012013

25. Wijaya K, Syoufian A, Fitroturokhmah A, et al. (2019) Chrom/nanocomposite ZrO_2-pillared bentonite catalyst for castor oil *(ricinus communis)* hydrocracking. *Nano Hybrids Compos* 27: 31–37. https://doi.org/10.4028/www.scientific.net/nhc.27.31
26. Liu B, He B, Peng HQ, et al. (2018) Unconventional nickel nitride enriched with nitrogen vacancies as a high-efficiency electrocatalyst for hydrogen evolution. *Adv Sci* 5: 1–7. https://doi.org/10.1002/advs.201800406
27. Xing Z, Li Q, Wang D, et al. (2016) Self-supported nickel nitride as an efficient high-performance three-dimensional cathode for the alkaline hydrogen evolution reaction. *Electrochim Acta* 191: 841–845. https://doi.org/10.1016/j.electacta.2015.12.174
28. Gillot F, Oró-Solé J, Palacín MR (2011) Nickel nitride as negative electrode material for lithium ion batteries. *J Mater Chem* 21: 9997–10002. https://doi.org/10.1039/c0jm04144k
29. Maya L (1993) Deposition of crystalline binary nitride films of tin, copper, and nickel by reactive sputtering. *J Vac Sci Technol A Vacuum, Surfaces, Film* 11: 604–608. https://doi.org/10.1116/1.578778
30. Pandey N, Gupta M, Stahn J (2021) Study of reactively sputtered nickel nitride thin films. *J Alloys Compd* 851: 156299. https://doi.org/10.1016/j.jallcom.2020.156299
31. Hasanudin H, Asri WR, Said M, et al. (2022) Hydrocracking optimization of palm oil to bio-gasoline and bio-aviation fuels using molybdenum nitride-bentonite catalyst. *RSC Adv* 12: 16431–16443. https://doi.org/10.1016/j.jallcom.2020.156299
32. Shalom M, Molinari V, Esposito D, et al. (2014) Sponge-like nickel and nickel nitride structures for catalytic applications. *Adv Mater* 26: 1272–1276. https://doi.org/10.1002/adma.201304288.
33. Shalom M, Ressnig D, Yang X, et al. (2015) Nickel nitride as an efficient electrocatalyst for water splitting. *J Mater Chem A* 3: 8171–8177. https://doi.org/10.1039/c5ta00078e
34. Ren JT, Wang YS, Song YJ, et al. (2022) Interface engineering of in−situ formed nickel hydr(oxy)oxides on nickel nitrides to boost alkaline hydrogen electrocatalysis. *Appl Catal B Environ* 309: 121279. https://doi.org/10.1016/j.apcatb.2022.121279
35. Xu K, Chen P, Li X, et al. (2015) Metallic nickel nitride nanosheets realizing enhanced electrochemical water oxidation. *J Am Chem Soc* 137: 4119–4125. https://doi.org/10.1021/ja5119495
36. Kreider ME, Gallo A, Back S, et al. (2019) Precious metal-free nickel nitride catalyst for the oxygen reduction reaction. *ACS Appl Mater Interfaces* 11: 26863–26871. https://doi.org/10.1021/acsami.9b07116
37. Hasanudin H, Rachmat A, Said M, et al. (2020) Kinetic model of crude palm oil hydrocracking over Ni/Mo ZrO_2–pillared bentonite catalyst. *Period Polytech Chem Eng* 64: 238–247. https://doi.org/10.3311/PPch.14765
38. Xi H, Li Q, Yang Y, et al. (2021) Highly effective removal of phosphate from complex water environment with porous Zr-bentonite alginate hydrogel beads: Facile synthesis and adsorption behavior study. *Appl Clay Sci* 201: 105919. https://doi.org/10.1016/j.clay.2020.105919
39. Munir M, Ahmad M, Mubashir M, et al. (2021) A practical approach for synthesis of biodiesel via non-edible seeds oils using trimetallic based montmorillonite nano-catalyst. *Bioresour Technol* 328: 124859. https://doi.org/10.1016/j.biortech.2021.124859
40. Huang W, Chen J, He F, et al. (2015) Effective phosphate adsorption by Zr/Al-pillared montmorillonite: Insight into equilibrium, kinetics and thermodynamics. *Appl Clay Sci* 104: 252–260. https://doi.org/10.1016/j.clay.2014.12.002

41. Wijaya K, Sugiharto E, Mudasir M, et al. (2010) Synthesis of iron oxide-montmorillonite composite and study of its structural stability againts sulfuric acid. *Indones J Chem* 4: 33–42. https://doi.org/10.22146/ijc.21871
42. Hasanudin, Said M, Faizal M, et al. (2012) Hydrocracking of oil residue from palm oil mill effluent to biofuel. *Sustainable Environ Res* 22: 395–400. Available from: https://www.researchgate.net/publication/287281979_Hydrocracking_of_oil_residue_from_palm_oil_mill_effluent_to_biofuel.
43. Moma J, Baloyi J, Ntho T (2018) Synthesis and characterization of an efficient and stable Al/Fe pillared clay catalyst for the catalytic wet air oxidation of phenol. *RSC Adv* 8: 30115–30124. https://doi.org/10.1039/c8ra05825c
44. Zhang X, Wang Z, Wang K, et al. (2021) Platinum modified nickel nitride catalyst on carbon nanotubes for energy conversion in alkaline medium. *Diam Relat Mater* 119: 108566. https://doi.org/10.1016/j.diamond.2021.108566
45. Ayodele OB, Togunwa OS, Abbas HF, et al. (2014) Preparation and characterization of alumina supported nickel-oxalate catalyst for the hydrodeoxygenation of oleic acid into normal and iso-octadecane biofuel. *Energy Convers Manage* 88: 1104–1110. https://doi.org/10.1016/j.enconman.2014.05.099
46. Olegario EM, Mark Pelicano C, Cosiñero HS, et al. (2021) Facile synthesis and electrochemical characterization of novel metal oxide/Philippine natural zeolite (MOPNZ) nanocomposites. *Mater Lett* 294: 129799. https://doi.org/10.1016/j.matlet.2021.129799
47. Yan LG, Qin LL, Yu HQ, et al. (2015) Adsorption of acid dyes from aqueous solution by CTMAB modified bentonite: Kinetic and isotherm modeling. *J Mol Liq* 211: 1074–1081. https://doi.org/10.1016/j.molliq.2015.08.032
48. Sadeghi S, Moghaddam AZ, Massinaei M (2015) Novel tunable composites based on bentonite and modified tragacanth gum for removal of acid dyes from aqueous solutions. *RSC Adv* 5: 55731–55745. https://doi.org/10.1039/c5ra07979a
49. Huang R, Zhang L, Hu P, et al. (2016) Adsorptive removal of Congo red from aqueous solutions using crosslinked chitosan and crosslinked chitosan immobilized bentonite. *Int J Biol Macromol* 86: 496–504. https://doi.org/10.1016/j.ijbiomac.2016.01.083
50. Vaýzoğullar AI (2017) Structure, Optical and photocatalytic properties of ZnO/CuO/bentonite nanocomposites in the oxidation of 2,6-dichlorophenol. *Theor Exp Chem* 53: 31–39. https://doi.org/10.1007/s11237-017-9498-6
51. Chen J, Zhu L (2009) Comparative study of catalytic activity of different Fe-pillared bentonites in the presence of UV light and H_2O_2. *Sep Purif Technol* 67: 282–288. https://doi.org/10.1016/j.seppur.2009.03.036
52. Anirudhan TS, Ramachandran M (2015) Adsorptive removal of basic dyes from aqueous solutions by surfactant modified bentonite clay (organoclay): Kinetic and competitive adsorption isotherm. *Process Saf Environ Prot* 95: 215–225. https://doi.org/10.1016/j.psep.2015.03.003
53. Tomul F (2011) Effect of ultrasound on the structural and textural properties of copper-impregnated cerium-modified zirconium-pillared bentonite. *Appl Surf Sci* 258: 1836–1848. https://doi.org/10.1016/j.apsusc.2011.10.056
54. Huo J, Min X, Wang Y (2021) Zirconium-modified natural clays for phosphate removal: Effect of clay minerals. *Environ Res* 194: 110685. https://doi.org/10.1016/j.envres.2020.110685.

55. Fatimah I, Nurkholifah YY (2016) Physicochemical and photocatalytic properties of Fe-pillared bentonite at various fe content. *Bull Chem React Eng Catal* 11: 398–405. https://doi.org/10.9767/bcrec.11.3.456.398-405
56. Amaya J, Suarez N, Moreno A, et al. (2020) Mo or W catalysts promoted with Ni or Co supported on modified bentonite for decane hydroconversion. *New J Chem* 44: 2966–2979. https://doi.org/10.1039/c9nj04878b
57. Vajglová Z, Kumar N, Peurla M, et al. (2019) Effect of the preparation of Pt-modified zeolite beta-bentonite extrudates on their catalytic behavior in n-hexane hydroisomerization. *Ind Eng Chem Res*. 58: 10875–10885. https://doi.org/10.1021/acs.iecr.9b01931
58. Huang R, Hu C, Yang B, et al. (2016) Zirconium-immobilized bentonite for the removal of methyl orange (MO) from aqueous solutions. *Desalin Water Treat* 57: 10646–10654. https://doi.org/10.1080/19443994.2015.1040849
59. Lin J, Jiang B, Zhan Y (2018) Effect of pre-treatment of bentonite with sodium and calcium ions on phosphate adsorption onto zirconium-modified bentonite. *J Environ Manage* 217: 183–195. https://doi.org/10.1016/j.jenvman.2018.03.079
60. Lin J, Wang H, Zhan Y, et al. (2016) Evaluation of sediment amendment with zirconium-reacted bentonite to control phosphorus release. *Environ Earth Sci* 75: 1–17. https://doi.org/10.1007/s12665-016-5744-9
61. Soliemanzadeh A, Fekri M (2017) The application of green tea extract to prepare bentonite-supported nanoscale zero-valent iron and its performance on removal of Cr(VI): Effect of relative parameters and soil experiments. *Microporous Mesoporous Mater* 239: 60–69. https://doi.org/10.1016/j.micromeso.2016.09.050
62. Kadeche A, Ramdani A, Adjdir M, et al. (2020) Preparation, characterization and application of Fe-pillared bentonite to the removal of Coomassie blue dye from aqueous solutions. *Res Chem Intermed* 46: 4985–5008. https://doi.org/10.1007/s11164-020-04236-2
63. Gage SH, Ruddy DA, Pylypenko S, et al. (2018) Deep eutectic solvent approach towards nickel/nickel nitride nanocomposites. *Catal Today* 306: 9–15. https://doi.org/10.1016/j.cattod.2016.12.016.
64. Wijaya K, Nadia A, Dinana A, et al. (2021) Catalytic hydrocracking of fresh and waste frying oil over Ni-and Mo-based catalysts supported on sulfated silica for biogasoline production. *Catalysts* 11: 1150. https://doi.org/10.3390/catal11101150
65. Hasanudin H, Asri WR, Andini L, et al. (2022) Enhanced isopropyl alcohol conversion over acidic nickel phosphate-supported zeolite Catalysts. *ACS Omega* 7: 38923–38932. https://doi.org/10.1021/acsomega.2c04647
66. Kurnia Amin A, Wijaya K, Trisunaryanti W (2018) The catalytic performance of ZrO_2-SO_4 and Ni/ZrO_2-SO_4 prepared from commercial ZrO_2 in hydrocracking of LDPE plastic waste into liquid fuels. *Orient J Chem* 34: 3070–3078. https://doi.org/10.13005/ojc/340650
67. Tye CT, Looi PY, Meow TL (2012) Hydroprocessing of crude palm oil to bio-diesel using mesoporous catalysts. *Adv Mater Res* 560–561: 538–543. https://doi.org/10.4028/www.scientific.net/AMR.560-561.538
68. Subsadsana M, Ruangviriyachai C (2016) Effect of NiW modified HZSM-5 and HY zeolites on hydrocracking conversion of crude palm oil to liquid hydrocarbons. *Orient J Chem* 32: 839–844. https://doi.org/10.13005/ojc/320208

69. Hasanudin H, Asri WR, Fanani Z, et al. (2022) Facile fabrication of SiO_2/Zr assisted with EDTA complexed-impregnation and templated methods for crude palm oil to biofuels conversion via catalytic hydrocracking. *Catalysts* 12: 1522. https://doi.org/10.3390/catal12121522
70. Francis J, Guillon E, Bats N, et al. (2011) Design of improved hydrocracking catalysts by increasing the proximity between acid and metallic sites. *Appl Catal A Gen* 409–410: 140–147. https://doi.org/10.1016/j.apcata.2011.09.040

AIMS Press